The deformation, strain hardening and wear behavior of chromium alloyed Hadfield steel in abrasive and impact conditions

Matti Lindroos[1)*], Marian Apostol[1)], Vuokko Heino[1)], Kati Valtonen[1)], Anssi Laukkanen[2)], Kenneth Holmberg[2)], Veli-Tapani Kuokkala[1)]

[1)] Tampere Wear Center, Department of Materials Science, Tampere University of Technology, P.O. Box 589, FI-33101 Tampere, Finland
[2)] VTT Technical Research Centre of Finland, P.O. Box 1000, FI-02044 VTT Espoo, Finland
[*]Corresponding author: matti.v.lindroos@tut.fi

ABSTRACT

The alloying of Hadfield steels aims at enhanced mechanical properties and improvements in the wear resistance. In this work, the impact and abrasive properties of a chromium alloyed high manganese Hadfield steel were experimentally studied using a wide variety of testing techniques and characterization methods. In addition, an in-service sample was characterized to identify the wear and hardening mechanisms in a real application (jaw crusher). The dynamic mechanical behavior of the steel was determined using the Hopkinson split bar technique. The abrasion properties were studied with three-body abrasion tests using several different natural abrasives. The effects of existing plastic strain and normal loading on the surface hardening and wear rate were further investigated with scratch testing. High velocity impact testing was performed to evaluate the effect of pre-strain on the impact wear behavior of the material.

It was shown that the dynamic loading affects both the yield behavior and the strain hardening rate of the studied steel. The connection between pre-strain, hardness and wear rate in abrasion was established. In impact conditions, plastic straining of the surface layer first has a positive effect on the wear resistance, but when strain hardening reached the observed ductility limit, it showed an adverse effect on the material's performance. The addition of chromium and an increase of the manganese content from the nominal ASTM Hadfield composition provided some improvements in the strength, ductility, and surface hardening of the studied steel.

Keywords: Hadfield manganese steel; Work hardening; High strain rate; Abrasive wear; Impact wear; Plasticity

1. Introduction

The use of Hadfield high manganese steels is still very popular in high stress impact-abrasive conditions, such as mining, due to its cost efficiency, ductility and ability to strain harden especially under impacts. Hadfield steels typically contain 10-14 wt.-% manganese and 1.0-1.4 wt.-% carbon [1]. In spite of their rather good mechanical performance, which is well established in many studies [2-6], to reach yield strengths in excess of 400 MPa while maintaining the strong strain hardening capability of the material with ductility values above 40% of plastic strain, alloying with elements like Cr, Mo, Si, Al, N, and V has been used to further enhance the properties of Hadfield steels to accommodate various conditions [1]. The alloying can provide improvements for example in strength and abrasion, corrosion, and impact resistance [7-11]. Composite structures containing Hadfield steel as a substrate material have also been shown to provide good overall wear performance [12]. However, especially in high strain rate conditions, i.e., at strain rates in the range of $10^3 \ldots 10^5$ s^{-1}, the mechanical behavior and wear resistance of high manganese steels may change

notably during operation, which should be accounted for in the design of the parts and components used for example in the mining machinery.

The addition of carbide forming elements is likely to enhance the abrasive resistance of high manganese steels, but it may also reduce their toughness due to the precipitation of grain boundary carbides. Moreover, alloying may drastically affect the deformation mechanisms by favoring slip, twinning or phase transformations from austenite to α' and/or ε martensite, depending on the stacking fault energy (SFE) of the alloy. Therefore, it is worthwhile to further investigate the mechanical behavior and wear properties of high manganese steels to obtain better understanding of their in-service performance and to further develop them.

In the mining conditions, materials often undergo both strong impacts and abrasion, which is a strong motivation to acquire more fundamental understanding of the wear, deformation and strain hardening behavior of various steels in high stress conditions. The deformation and wear occurring in mineral crushers can be divided into two major categories *i)* high stress and high strain rate impact-like deformation of the steel surface when rocks hit the surface and are crushed, and *ii)* high stress abrasion caused by large and crushed rocks sliding on the surface.

In this work, both abrasive and impact wear behavior of a chromium alloyed high manganese austenitic wear resistant steel were studied. The mechanical behavior and hardening of the steel were investigated using high strain rate compression tests that describe the rock impact and rock crushing stages. Multi-scale abrasion tests were used to evaluate the wear resistance of the test material against sliding abrasives in the laboratory scale. The crushing pin-on-disk setup was used to study the material's wear resistance and hardening behavior against natural rock abrasives. In the controlled single asperity scratch test a rigid indenter slides on a clean surface and provides information for example on the effects of the deformation history of the material and its relationship to the surface hardening. The impact wear of the hardened surface was investigated using high velocity single impact experiments. The results of this work will also be used to evaluate the material's general performance and to provide basic material data for numerical simulations.

2. Materials and methods

2.1 Microstructure and mechanical testing

The studied high manganese wear resistant steel contains 16.5 wt.-% manganese and 1.15 wt.-% carbon. Thus, the amount of manganese is slightly higher than in the standard grades [1]. Moreover, the steel used in this work is alloyed with 1.8 wt.-% chromium, the effects of which on the impact and abrasive resistance of the material are also experimentally studied. The material was cast, quenched and annealed, and as a result it contained some cast imperfections in the microstructure. The austenitic microstructure had the coarse grain size of 200-800 µm. The bulk hardness in the as-cast state was 250 - 300 HV5.

To study the performance of the hardened surface in the laboratory scale and the effect of pre-strain on the steel behavior, cylindrical steel samples with a diameter of 8 mm were pre-compressed to plastic strains between 0…40%. The samples were first mounted in a resin to ensure proper sample fixing in the experimental equipment and to provide sufficient support for the samples. The compression strain rate in the pre-straining was set to a constant value of 0.1 s^{-1}. The large cylindrical samples having a 36 mm diameter used in the crushing pin-on-disk tests were not plastically pre-strained.

The mechanical testing was performed with a servo-hydraulic materials testing machine in compression at the quasi-static strain rates of $10^{-3}…10^{-1}$ s^{-1}. The Hopkinson split bar (HSB) at Tampere University of Technology [13] was employed for the dynamic high strain rate tests. All experiments were performed at room temperature. The higher strain rates covered the range of 1500 to 4000 s^{-1} describing the impact conditions in mineral crushers. Additional tensile tests at quasi-static strain rates were carried out to determine the failure strength and the hardness of the material at failure. Dynamic tensile tests were also performed with a tensile Hopkinson bar setup at 1500 s^{-1} to provide additional failure properties.

2.2 Abrasion experiments

Three-body abrasive wear tests were performed with the crushing pin-on-disk device developed at Tampere Wear Center [14]. Figure 1 presents the setup, in which abrasives are placed between the sample pin and the bottom disk. When the bottom disk rotates at 28 rpm, the pin is pneumatically pressed against a bed of gravel with a force of 235 N for 5 seconds and then lifted up for 2.5 seconds. In the next cycle, the pin comes again into contact with the pile of gravel ensuring sufficient amount of abrasives in the contact. The contact area of the pin was 1000 mm^2. During a 30 minute wear test, the weight of the sample is measured every 7.5 minutes. When the test advances, the abrasive is comminuted progressively into finer particles. The test samples were pre-worn for 15 minutes with 2-4 mm granite abrasive to ensure a similar surface for all samples and to minimize the effect of sharp edges of the cylindrical pin sample. Moreover, the pre-wearing done with real abrasives ensures that the test material is hardened in a similar manner as in the in-service conditions before the actual wear test commences. Table 1 presents the selected size distribution of the screened abrasives, which was chosen to produce the maximum amount of wear in the tests. The abrasives were granite, quartz, tonalite, and basalt. The bottom disk used in the experiments was made of a 600 HV tool steel. The amount of wear in the crushing pin-on-disk experiments was determined from the mass loss measurements conducted intermittently during the test.

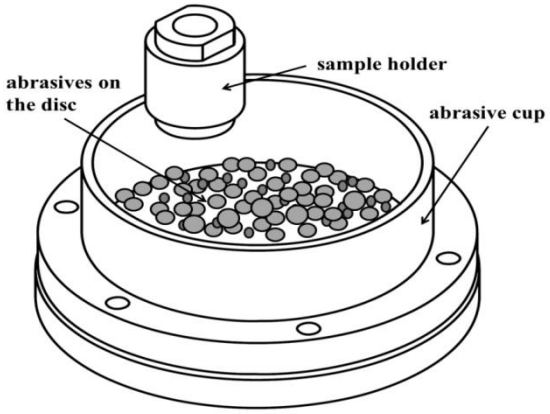

Figure 1. Crushing pin-on-disk experimental setup.

Table 1. Size distribution of the abrasives in the crushing pin-on-disc tests.

Size [mm]	Amount [g]
8-10	50
6.3-8	150
4-6.3	250
2-4	50

The scratch tests were performed with a standard rigid Rockwell-C tip having a radius of 200 µm ± 10 µm using the CETR UTM-2 tribometer. To study the effects of pre-strain on wear and work hardening, single scratch tests were performed at four constant loads of 20 N, 40 N, 60 N, and 80 N. The sliding velocity was kept constant at 0.1 mm/s. To further investigate the continuous wear of hardened surfaces corresponding to a crusher jaw, multiple scratches overlapping each other were run on in-service samples using 1, 2, 5, and 10 cycles and moderate 40 N and high 80 N normal loads. The surface hardness of the tested samples was measured from the bottom of the scratch grooves with a sufficiently small weight (HV0.2) to avoid interference with the ploughed ridges and to ensure contact at the nominally flat bottom of the scratch groove.

2.3 High velocity single impact experiments

High velocity single impact tests were performed in order to study the effect of pre-strain on the wear and failure behavior of the material. The impact tests were carried out with the High Velocity Particle Impactor (HVPI) at Tampere Wear Center [15,16]. The device has a 9 mm non-rifled (smoothbore) gun barrel that fires the projectile towards a fixed target placed at a 1 m distance using pressurized air. A hard metal WC-Co ball of 9 mm in diameter and 0.569 g in weight was used as a projectile. The target sample was tilted at a 30 degree angle relative to the barrel of the gun. Two impact velocities were chosen, 45 ±1 and 76 ±1 m/s, corresponding to the impact energies of 6 J and 17 J, respectively. The impact events were recorded with a high speed camera at a 50 µs interframe rate.

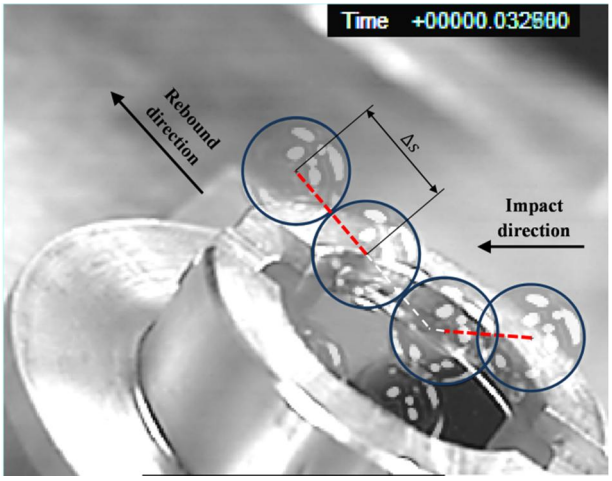

Figure 2. Four stages of the impact incident on a sample at a 30 degree angle recorded with a high speed camera. The outlines of the projectile are shown for clarity.

The initial kinetic energy of the projectile was calculated using the initial velocity, v_{init}, measured with a chronograph placed in front of the sample. The exit velocity of the projectile, v_{exit}, was calculated from the high speed images by determining Δs, which is the distance travelled by the centroid of the projectile, and Δt, the time elapsed between the images used in the velocity determination. Accordingly, the fraction of dissipated energy, E_d, was calculated as:

$$E_d = \frac{1}{2} m_p (v_{init} - v_{exit})^2 \quad (1)$$

where m_p is the mass of the projectile.

2.4 Characterization

The material removal, defined as volume loss taking place in the scratch and impact experiments, was characterized with optical profilometry. The wear marks were measured with Veeco NT-1100 profilometer and analyzed numerically using a special Matlab code.

The hardness values were measured as Vickers hardness (HV). After the crushing pin-on-disk wear tests, the surfaces were characterized optically and the surface hardness values of the samples were measured using the weight of one kilogram (HV1) not to penetrate excessively deep into the undeformed subregions. The severity of plastic deformation and its relationship to wear was estimated using the cutting-to-plasticity ratio φ determined from the 3D surface profiles, as presented in Equation 2

$$\varphi = \frac{|V_{neg}| - |V_{pos}|}{|V_{neg}|} \quad (2)$$

where V_{neg} is the negative volume below the undeformed (zero) level and V_{pos} is the positive volume above it. When the value of φ reaches 1, all material has been cut off, while 0 denotes ideal plastic flow where material is only displaced but not removed.

3. Results

3.1 Surface hardening and damage mechanisms in the in-service sample

The surface hardening and wear surfaces were characterized from the samples cut from a worn jaw of a jaw crusher. Figure 3a shows the cross-section of the worn and heavily deformed surface after severe use in the crusher. The zone of heavy plastic deformation has clearly extended deep into the microstructure, as seen from the intense slip bands in the surface and subsurface grains. The deformation in the austenite grains manifests itself also as twins, which are formed during heavy deformation and partly explain the strong strain hardening of the high manganese alloys. The main reason for the extensive twin formation in these alloys is that manganese increases the stacking fault energy which, in turn, favors twinning over martensitic transformation under heavy mechanical loading.

Figure 3b presents both abrasive cutting marks and impact craters on the rough surface profile. In general, the impacts during the crushing sequence induce hardening. On the other hand, the impacts may also generate large wear particles, which appear as dents and craters on the surface, when the surface is no longer able to accommodate the impact energy by plastic deformation. The abrasion occurring after the compressive crushing phase scrapes material off from the surface, which effectively increases the wear rate if the surface is not sufficiently hardened.

The presence of carbides at the grain boundaries may generally increase the abrasion resistance of the austenitic microstructure. However, carbides often generate stress concentrations and are thus susceptible to initiate failure. In the cross-section (Fig. 3a), some visible fractures along the grain boundaries can be observed from the surface. This indicates that grain boundary cracking is one of the failure mechanisms of the surface.

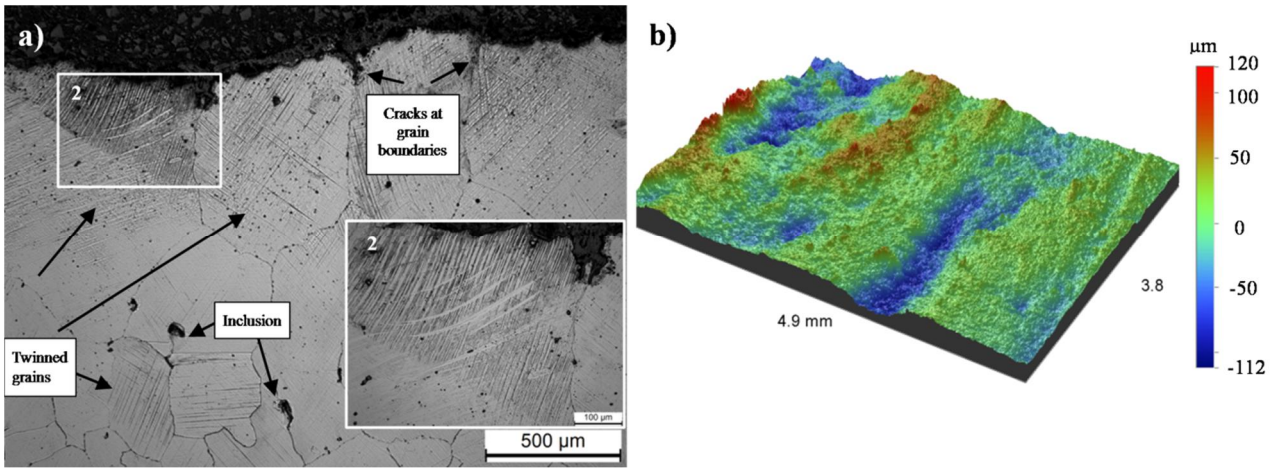

Figure 3. a) Cross-section of the deformed steel and b) wear surface profile showing damage generated by impacts and abrasion in the in-service sample.

The average hardness profile of the cross-section in Figure 4 demonstrates the effective depth of plastic deformation and the maximum hardening capability of the steel, which generally depend on the nature of the abrasives crushed in the application. The bulk hardness was reached at about 7 mm from the surface. The maximum hardness, roughly 680-720 HV, was measured from the sub-surface region, which basically covered only one grain layer due to the large grain size. Below this layer, the hardness relatively quickly reduced to 550-650 HV. The heavily twinned surface layer is clearly visible in Figure 3a.

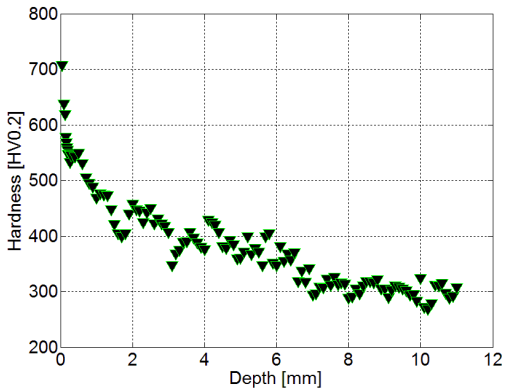

Figure 4. Hardness gradient measured from the cross-section of the in-service sample.

3.2 Dynamic hardening and strain-hardness relationship

Figure 5 illustrates the compressive true stress - true plastic strain curves of the as-cast high manganese steel samples in a wide strain rate range at room temperature. The curves and data shown in Fig 5a are slightly smoothed for clarity. The yield strength of the material increases in the well-established manner throughout the studied strain rate range, but as Fig 5b shows, the strain hardening rate θ $(= \partial\sigma/\partial\varepsilon)$ depends on the strain rate in a more complex manner. At quasi-static strain rates, also the strain hardening rate increases until 10^{-1} s^{-1}, after which the adiabatic heating due to the increasing plastic deformation and relatively poor thermal conductivity of the Hadfield steels starts to increase the material temperature, thus decreasing the thermal component of the flow stress. As increasing temperature also increases the stacking fault energy, this may have an effect on the twinning propensity of the material, but based on the upward concave shape of all determined

stress-strain curves, twinning still works as a hardening mechanism even at the higher strain rates. In addition, strain rate as such may affect the twinning behavior of high manganese steels, but its possible effect cannot be determined from the current data. As seen in Figure 5a, adiabatic heating leads to a situation where the 0.1 s^{-1} and 1 s^{-1} curves intersect already at the plastic strain of about 12%. In the dynamic strain rate range of 1500…4000 s^{-1}, the strain hardening rate increases again with increasing strain rate but stays below the values seen in the quasi-static region. It should, however, be pointed out that the dislocation dynamics in the quasi-static and dynamic strain rate regions are different, the former being governed by the thermally activated dislocation motion and the latter by the various dislocation drag mechanisms, and therefore a direct comparison of the strain hardening rates in these two regions is not possible.

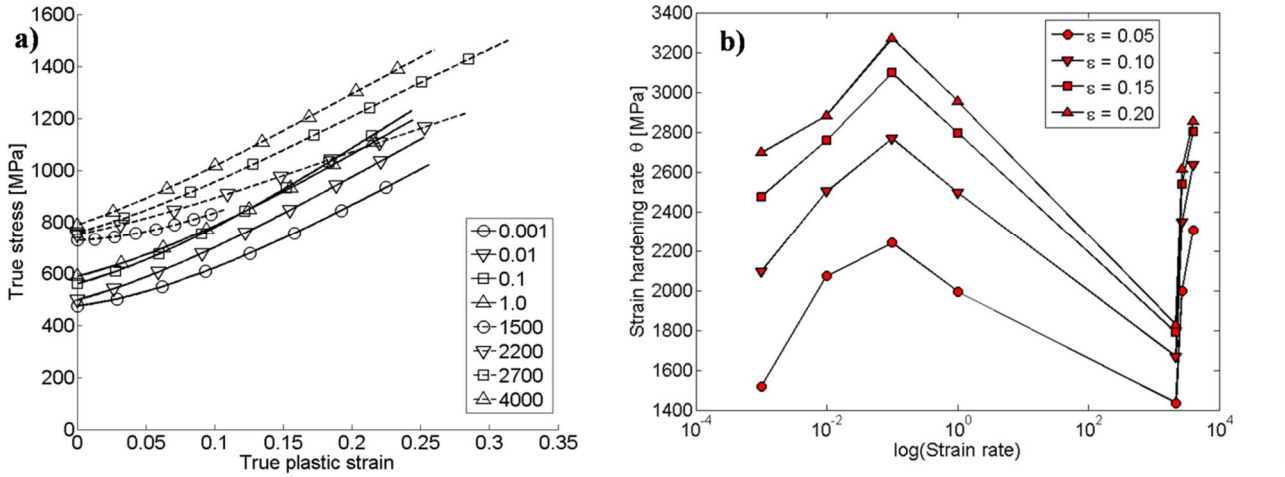

Figure 5. a) Stress-strain behavior of the studied high manganese steel at various strain rates in compression. The samples did not fail during the tests. b) The strain hardening rate as a function of strain rate at various constant plastic strains.

Figure 6 presents the tensile stress-strain curve at 10^{-1} s^{-1} up to fracture together with the hardness of the pre-strained samples. The highest HV0.2 hardness, roughly 700±20 HV, was measured both from the tensile specimens near the fracture and also directly from the wear surface of the in-service samples. Thus, to approximate the maximum surface strain ε_{max} before failure, the fitted hardness-strain curve in Figure 6 was extrapolated to the point of maximum tensile stress of the experiment, i.e., $\sigma_T \sim 1550$ MPa at $\varepsilon_{max} \sim 0.51$. Realistically it is quite impossible to know the exact strain state of the surface layer, and therefore according to this indirect approximation procedure, the strain maximum is considered to be the maximum tensile strain of the in-service samples studied in this work.

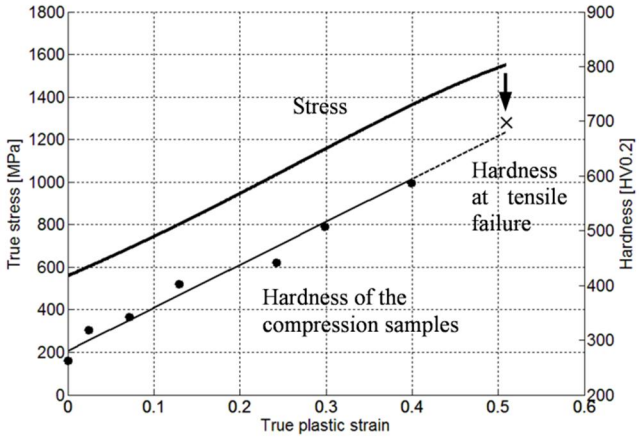

Figure 6. Tensile stress-strain behavior and its relationship to the hardness of pre-strained samples.

Further high strain rate testing was attempted with the tensile Hopkinson bar. The curve obtained at the maximum strain rate of 1500 s^{-1} showed very similar behavior to the ones seen in Figure 5. Clearly higher yield strengths, 660-700 MPa, were achieved, but the strain hardening rate was lower than in the quasi-static case seen in Figure 5. Thus, the failure strength at 1500 s^{1} was rather similar to the low strain rate case, i.e., σ_T ~ 1585 MPa at ε_{max} ~ 0.56.

3.3 Crushing pin-on-disk abrasion experiments

Figure 7 presents the total mass losses of the crushing pin-on-disk tests with four different rock types. The composite hardness of the rocks varied from less than 500 HV to over 1100 HV. The results indicate that an increase in the rock hardness has only a limited increasing effect on wear and that the rock abrasiveness values correlate better with the mass loss results. The highest mass loss in the studied steel was produced by tonalite with the high hardness and highest abrasiveness.

The crushabilities of basalt, granite, tonalite and quartz were 24%, 34%, 27% and 74%, respectively. A low crushability index indicates that the rock is not easily crushed into smaller particles. For example, the high crushability of quartz seems to reduce the mass losses in spite of the quite high hardness and abrasiveness of the rock. In contrast, basalt rocks appeared in very flake-like shapes both before and after the experiments, which is in good agreement with the low crushability index. However, due to its low hardness and low abrasiveness, basalt caused the lowest amount of wear on the steel surface. These results indicate that the most marked effects on wear are related to abrasiveness and hardness accompanied by a smaller effect of crushability.

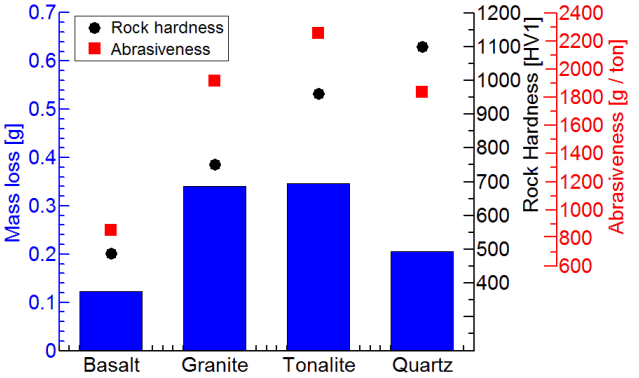

Figure 7. Crushing pin-on-disk wear results with four different abrasives together with the average hardness of the different rock types and abrasiveness values.

The surface hardness values of the test material are presented in Figure 8. The in-service surface hardness was measured directly from a sample taken from a crusher, both from the rough wear surface and from a slightly polished surface. The surface hardness of the 40% pre-strained sample was measured in the compression direction.

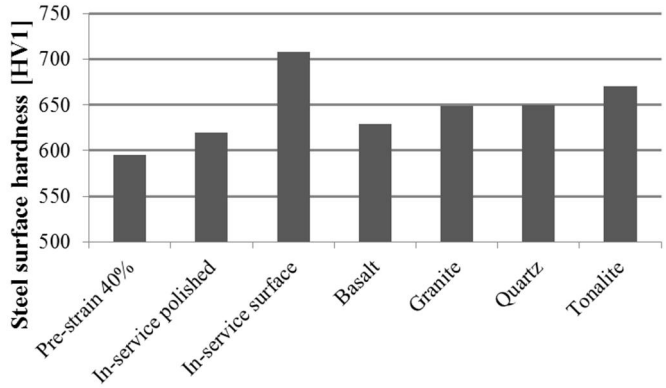

Figure 8. Hardness of the steel samples after the crushing pin-on-disk experiments with four rock types and after 40% pre-strain, measured directly from the in-service wear surface and from a slightly polished in-service surface.

The highest surface hardness in the crushing pin-on-disk experiments was produced by tonalite. It is noticeable that the hardness values are all quite high and close to the average hardness values measured from the in-service sample surface. This implies that the steel surface undergoes quite considerable hardening from the bulk hardness of 250-300 HV, thus showing less substantial dependence on the hardness of the abrasives. It should, however, be taken into account that all of the tested abrasives had a hardness higher than the bulk hardness of the steel.

3.4 Single and multiple scratch tests and surface hardening

The effect of loading on wear and its dependence on the current plastic strain state of the surface were assessed with single scratch experiments using four normal loads. The wear rates are presented as volume loss per sliding distance in Figure 9. The pre-strain has a decreasing effect on wear, which is caused by the increasing hardness of the material (see Fig. 6). The optical inspection of the scratches showed that the samples with lower pre-strain and lower hardness exhibited more ploughing-like behavior due to the larger deformations (i.e., material is pushed aside) in the groove as a function of normal load. Although the depth and width of the grooves decreased with larger pre-strains and in the in-service samples, a clear increase in cutting was observed. For example, in the samples pre-strained for 40% as well as in the in-service samples an increase in the cutting-to-plasticity ratio φ from 0.26-0.35 to 0.5-0.6 indicates that material was more efficiently removed than just displaced. This manifested itself as long and narrow wear particles removed from the ridges.

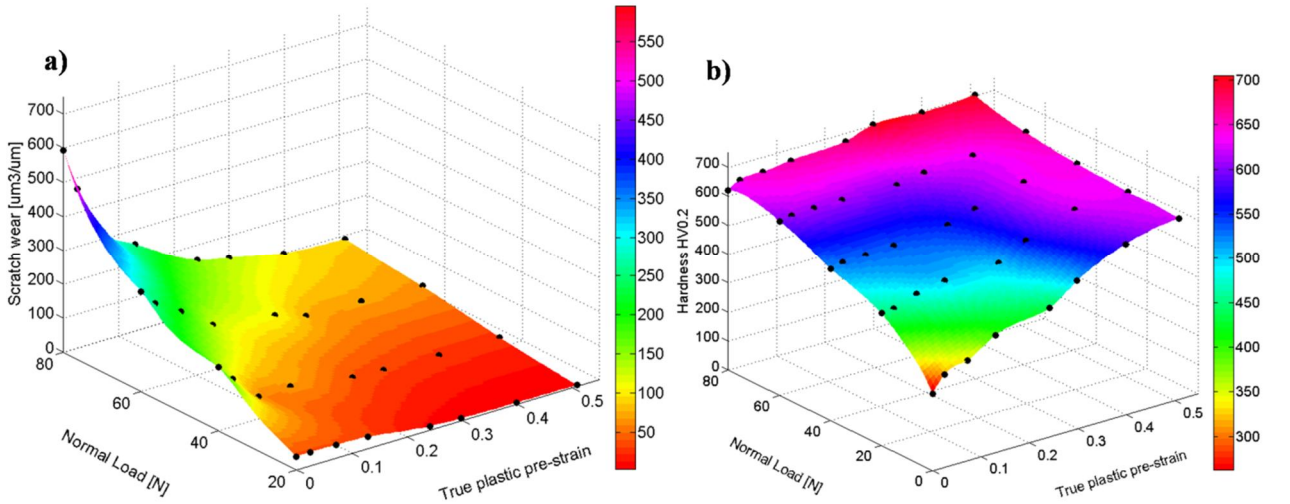

Figure 9. a) Volume loss per sliding distance at four normal loads for various pre-strains presenting the effect of surface hardening on scratch wear rate, b) Surface hardening caused by scratching at various pre-strains and normal loads. The hardness values were measured from the bottom of the scratch grooves after the experiment.

Figure 9b presents the hardness values after the scratch tests as a function of normal load and the amount of deformation after pre-straining. The measured hardness values of 650-700HV after the high normal load experiments correlate well with the ones found in Figure 6 at fracture.

The coefficient of friction during the experiments increased as a function of normal load but at the same time followed quite well the changes in hardness. For example, when the surface hardness increased from 250 HV to 700 HV, the coefficient of friction decreased from 0.19 to 0.07 at the normal load of 40 N. As an exception, in the case of the in-service sample scratched at high normal loads, the surface was no longer able to deform leading to the formation of wear particles that increased the value of the coefficient of friction. In most cases, higher normal loads and thus slightly higher surface pressures also resulted in higher friction values, although it should be noted that the rigid diamond indenter is not a direct comparison to the natural rocks with varying geometries and local properties.

Figure 10 presents the results of cyclic scratch tests performed on polished in-service samples at constant normal loads of 40 N and 80 N. The specific wear energies are calculated as volume losses divided by the normal force times the sliding distance. The results show a clear decreasing trend as a function of scratch cycles. The increase in surface hardness is not likely the only reason for this behavior as the hardness close to 700 HV is reached already after a few cycles. In the first cycle the wear volume is the highest because the groove is formed on a fresh polished surface. The following load cycles remove the partly loose wear particles from the ploughed side ridges. The visual inspection confirmed that approximately after five cycles the wear of the ridges is more constant and it no longer acts as an accelerating component. The coefficient of friction did not change noticeably when the normal load was increased from 40N to 80N, indicating that there was no essential change in the wear mechanism.

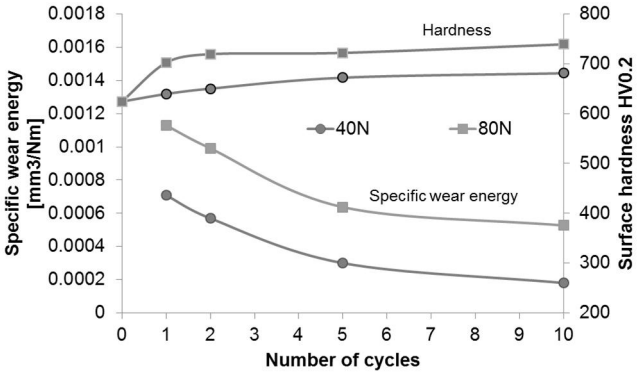

Figure 10. Specific wear energy and surface hardening of in-service samples in the overlapping multiple scratch tests at 40 N and 80 N.

3.5. High velocity impact experiments

Figure 11 presents the volume loss results of oblique single high velocity impacts for four pre-strains and for the in-service samples. The dissipated fraction of the two initial impact energies of 6 J and 17 J varied between 30…40 %. Thus the energy transferred to the sample (as deformation, heat, friction, etc.) at a 30 degree impact angle is only a fraction of the total energy of the projectile. No clear connection between the pre-strain and the energy dissipation during the contact was found. However, the connection between wear and energy dissipation was evident. When the volume loss was scaled by the used energy, the 6 J or 17 J curves appeared very similar when the pre-strain was kept constant. This implies that there is a strong connection between the used energy and wear within the current test range. The cutting-to-plasticity/ploughing ratio, that may be linked to a change in the wear mechanism, showed clearly more cutting when the volume loss started to increase.

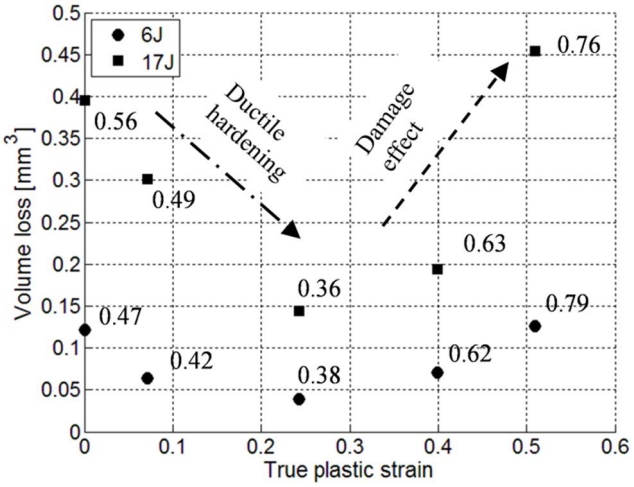

Figure 11. Volume loss measured from the surface after 6 J and 17 J single impacts at four pre-strains and from the hardened in-service samples at a 30 degree impact angle. The numbers represent the cutting-to-plasticity ratios at each data point.

A microscopic study on the craters revealed marked amounts of fractures along the grain boundaries even quite far away (~1-2 times the crater length) from the crater. Also, the ploughed end of the crater suffered from substantial deformation and removal of large wear particles. The bottoms of the craters showed only slight adhesion marks generated between the sample material and the impacting ball, indicating rather low friction conditions. The microhardness measurements in the

vicinity of the crater showed the highest values of around 700 HV near the edge of the crater. When moving away from the heavily deformed area, the hardness decreased quite rapidly, mostly within a distance of one crater length.

Figure 12 shows the cross-section of an impact crater on an in-service sample after an impact at 17 J. The damage has developed even further away from the actual impact site and propagated as a subsurface network almost down to the depth of 5 mm. The location of the crack network is at the ploughed end of the crater. It is expected that this region suffers from remarkably high shear stresses during the impact and especially when the projectile is reflected away from the surface.

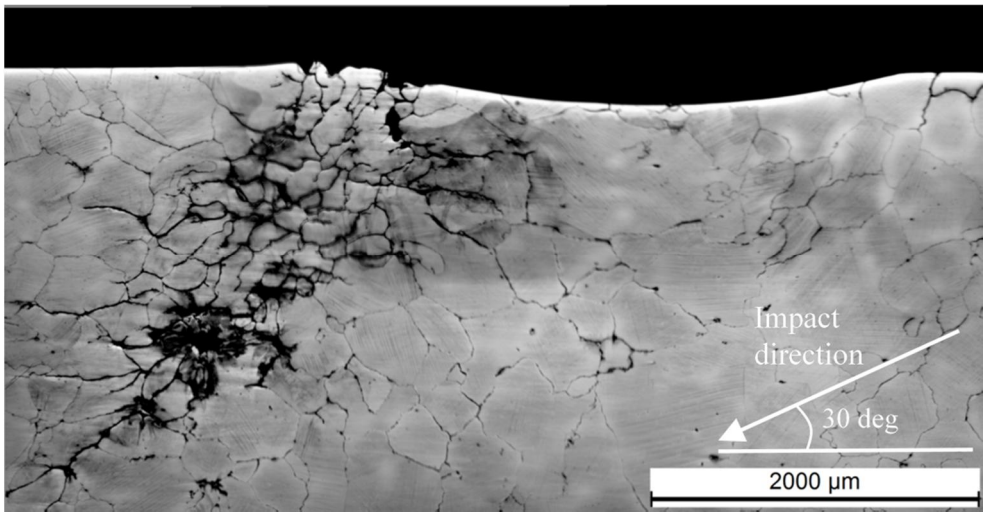

Figure 12. Cross-section of the impact crater. The arrow indicates the impact direction.

4. Discussion

The abrasive and impact wear behavior of Hadfield steels has been discussed in many papers, such as [11,17,18,19]. However, the high strain rate stress-strain behavior of these steels has not been so widely and precisely studied, and therefore it is not quite clear why the alloys sometimes respond to impact loadings in a different manner. The high strain rate Hopkinson Split Bar experiments conducted in this work show that the yield strength of the chromium alloyed Hadfield steel increases from about 480 to 785 MPa when the strain rate is increased from the quasi-static region to 4000 s^{-1} at room temperature.

The upward (concave) curvature of the stress-stain curves of the studied high manganese steel, as seen in Figure 5a, indicates that the strain hardening observed in this material is caused also by other strain (or stress) dependent microstructural features than dislocations and their interactions, such as strain/stress induced twins [5, 20-24]. In the optical microscopic studies, the high strain rate samples showed notably more grains with high number of localized slip lines and twins than the quasi-static samples, but it was also observed that the distribution and spacing of such grains was less uniform in the high strain rate than in the quasi-static samples. These observations were confirmed by microhardness measurements, which revealed locally higher hardness values in the high strain rate samples than in the quasi-static ones at similar amounts of average strain.

The strain hardening in high manganese steels can take place by common dislocation interactions as well as by twinning and phase transformations and their interactions with moving dislocations,

depending on the alloying, stacking fault energy, and texture of the material [19-28]. In addition, as observed in this study, the strain rate seems to affect the mechanical twinning propensity and thus the strain hardening behavior of Hadfield type steels by increasing the density of twins in individual grains with increasing strain rate. Some studies on the twinning-induced plasticity (TWIP) steels [30-32], however, report the adiabatic heating to increase the stacking fault energy so much that mechanical twinning may cease completely, leading to pure dislocation interaction based strain hardening of the material or, in some cases, to thermal softening if the remaining hardening effect cannot compensate for the effect of increasing thermal activation on the required flow stress of the dislocations. Due to the rather low thermal conductivity of the Hadfield steel (around 10-15 W/mK), the adiabatic conditions are achieved already at quite low strain rates similarly to austenitic stainless steels. For example, by assuming fully adiabatic conditions and 95 % generation of heat from the conducted deformation work (the rest being stored in microstructural defects such as dislocations), the estimated macroscopic increase of temperature during the high strain rate experiments of Fig 5a would be 52, 72, 91, and 75 ℃ for the strain rates of 1, 2200, 2700 and 4000 s^{-1}, respectively. For example in TWIP steels, such increases in temperature can already cause an increase as high as 10-25 mJ/m^2 in the stacking fault energy [34,35].

The inhomogeneous hardening of the microstructure may also cause stress concentrations in the microstructure, which can further promote the grain boundary fractures related to the grain boundary carbides due to chromium alloying. However, no direct evidence of increased brittleness at high strain rates was found in this work to confirm this.

Recently Wen et al. [10] have used silicon alloying in high manganese austenitic steels to increase the strain hardening rate. They have reported a rather notable decrease of 30% in the yield strength of a silicon alloyed steel compared to the 350 MPa of the conventional Hadfield steel. More importantly, however, with silicon alloying the flow stress of 1100 MPa has been achieved already at 0.2 of plastic strain instead of the over 0.25 strain of the conventional Hadfield. However, the usability of this alloy in mining conditions may be limited because of the lowered ductility. For comparison, the currently studied steel had the yield strength of 480 MPa and the flow strength of 950 MPa at 0.2 strain when tested at a low strain rate. Besides the slightly lower strain hardening capability of the currently studied alloy, the tensile failure strains of over 0.5 in both quasi-static and high (1500 s^{-1}) strain rates are markedly higher than reported in other studies [10,11,29]. This may be beneficial in fatigue and impact conditions typically encountered in mineral crushing.

To extend the considerations to real abrasives, the crushing pin-on-disk results showed interesting features. First of all, the abrasion resistance of the steel depended greatly on the abrasives in use. However, there seems to be no single abrasive property that correlates with the wear rate. For example, hardness of the rock is not sufficient alone to explain the changes in the wear rates - in fact, the values of abrasiveness and crushability provided much better correlation with wear. This is mainly because the hardness of the abrasive does not directly provide information about the fracturing of the rocks. For example, when the rock fractures to plate-like or round particles, the result is quite different regardless of the similar hardness, as was seen with quartz and tonalite. Moreover, the surface hardening of the studied steel depended on the rock strength and crushability. If the rocks only become rounder and do not fail very easily under the crushing forces, the steel surface undergoes more severe deformation thus leading to higher strain hardening. This phenomenon and its effect on the increased surface hardness were observed in the screening of the abrasives after the tests. Tonalite particles had remained larger in size than the other tested rocks. In contrast, if the abrasive fractures easily but has a high hardness, alloys with more rapid strain hardening could provide better abrasion resistance as the maximum hardness would be obtained already at lower strains [10,11,29]. In other words, these alloys offer better surface hardness to

abrasive hardness ratio already at low surface strains. On the other hand, that kind of alloys would most likely exhibit higher wear rates than the more ductile alloys under continued impacts.

The observations of El-Mallawi et al. [9] on the effect of added chromium on the abrasion, corrosion and impact resistance of 10-14 Mn Hadfield steels are in a good agreement with the current results. According to the experiments of El-Mallawi et al. [9], the conventional Hadfield grade (1.13-C, 10-Mn) has a relatively good abrasion resistance and noticeable surface hardening even in pure abrasive conditions. However, when combined impact-abrasion conditions or corrosive environment are present, the chromium alloyed grades provide even better wear resistance. In addition, roughly 150-200 HV higher hardness values were measured from the abraded surfaces of the currently investigated steel compared with the earlier studies [9]. The grade studied in this work has a similar amount of chromium as that studied by El-Mallawi et al. [9] but contains more manganese in the composition. The effect of manganese is not straightforward, often due to the presence of other alloying elements, but for example in TWIP steels manganese is used 15-30% to stabilize austenite and to adjust the stacking fault energy to a desired level [22,36,37]. In Hadfield steels, maintaining a suitable content of both Mn and C is important for the same reasons, especially for obtaining a desired SFE for example for mechanical twinning in the presence of other SFE affecting alloying elements such as aluminum, nitrogen, and chromium [7, 38-40].

The single grit scratch tests were used to study the effects of pre-strain and normal load on the hardening and wear rates. The obtained results may also be used as material data for simulation purposes. The use of a rigid indenter instead of natural rocks eliminates the possible failure of the indenting tip or changes in its geometry and allows better analysis of the actual wear and surface hardening behavior. Even though hardening from the bulk hardness of 250-300 HV to the maximum hardness of 700 HV was obtained at nominal strains of 0.5 (approximated from Figure 6), the surface did not show any signs of brittleness even at high plastic pre-strains and/or high loads. In the multiple scratch tests it was rather surprising that doubling the load from 40 N to 80 N did not have any significant effect on the wear mechanism, although it more or less doubled the wear rate. This suggests that probably no notable hardening occurred anymore, because the surface hardness had already more or less reached its maximum value. The surface that was exposed after the removal of the topmost hardened layer was therefore capable of providing sufficient ductility and also showed the required ability to strain harden and to resist abrasion under the applied high surface pressures.

The high velocity impact experiments showed that the plastic pre-strain does have a decreasing effect on wear until a certain limiting value of deformation has been reached. Increase in the cutting-to-plasticity ratio was generally observed above 30 % of plastic strain. This indicates that the surface starts to behave in a less ductile manner and releases wear particles by cutting rather than ploughs material aside by pure plastic deformation. The highest microhardness values were measured for the grains that were twinned at the crater edges. Moreover, notable amounts of grain boundary cracks were developed during the impact and directed from the crater to the less deformed areas. This may indicate a slight embrittling effect caused by chromium. Similarly, the subsurface crack networks were developed reaching significant depths. However, it could not be confirmed whether the crack networks would cause a marked weakening effect in the in-service samples.

5. Conclusions

An experimental study on the mechanical and wear behavior of a chromium alloyed high

manganese austenitic steel was conducted using several different research techniques. The aim of the work was to elucidate the high strain rate and impact behavior of the steel and to obtain better understanding of its abrasive and impact wear behavior in different deformation states. The following observations and conclusions were made in this study:

1) The chromium alloyed high manganese austenitic steel is more resistant to deformation during dynamic events such as impacts than during quasi-static loading. Increasing strain rate increases the material's yield strength in the whole studied strain rate range but affects the strain hardening rate in a more complex manner. In the quasi-static region, also the strain hardening rate increases until adiabatic heating sets in at around 1 s^{-1}. In the high strain rate region, the strain hardening rate increases again with increasing strain rate, and intense twinning is observed in some of the grains. At low strain rates in the quasi-static region, twinning is less frequent but more uniform, as also the hardness measurements indicate.
2) The abrasive wear behavior of the studied steel depends on the properties of the abrasive, such as hardness, abrasiveness and crushability. The maximum surface hardness of the steel cannot be obtained in pure abrasion conditions, such as in the experiments with the crushing pin-on-disk used in this work. This indicates that the steel requires a decent amount of impacts for maximum strain hardening and to perform in the best possible manner.
3) Prior deformation promotes twins in the microstructure and increases the wear resistance in an abrasive environment due to the increased hardness of the surface. Higher surface loads cause the surface hardening to occur more rapidly.
4) Below 0.3 of plastic strain, the pre-strain has a wear decreasing effect against impacts. Above this limit, however, the surface behaves in an increasingly brittle manner. The highest wear rates and increasing amounts of grain boundary fractures were observed at total plastic strains of around 0.5 at the surface, near the tensile strain limit of the material.

Acknowledgements

This study was a part of the FIMECC DEMAPP program funded by Tekes and the participating companies.

References

[1] ASTM A128/A128M, Standard Specification for Steel Castings, Austenitic Manganese, (2012).

[2] Dastur, Y.N., Leslie, W.C.: Mechanism of work hardening in Hadfield Manganese steel, Metall Mater Trans A. 12, 749-759 (1981).

[3] Adler, P.H., Olson, G.B., Owen, W.S.: Strain hardening of Hadfield manganese steel, Metall Mater Trans A. 17, 1725-1737 (1986).

[4] Owen, W.S., Grujicic, M.: Strain hardening of austenitic Hadfield manganese steels. Acta Mater. 47, 1, 111-126 (1999).

[5] Karaman, I., Sehitoglu, H., Gall, K., Chumlyakov, Y.I., Maier, H.J.: Deformation of single crystal Hadfield steel by twinning and slip. Acta Mater. 48, 1345-1359 (2000).

[6] Bayraktar, E., Khalid, F.A., Levaillant, C.: Deformation and fracture behaviour of high manganese austenitic steel. J. Mater. Process. Technol. 147, 145-154 (2004).

[7] Canadinc, D., Karaman, I., Sehitoglu, H., Chumlyakov, Y.I., Maier, H.J.: The Role of Nitrogen on the Deformation Response of Hadfield Steel Single Crystals. Metall Mater Trans A. 34, 1821-1831 (2003)

[8] Zuidema, B.K., Subramanyam, D.K., W.C., Leslie.: The effect of aluminum on the work hardening and wear resistance of hadfield manganese steel, Metall Mater Trans A. 18, 9, 1629-1639 (1987).

[9] El-Mallawi, I., Abdel-Karim, R., Naguib, A.: Evaluation of effect of chromium on wear performance of high manganese steel. J. Mater. Sci. Technol. 17, 1385-1390 (2001).

[10] Wen, Y.H., Peng, H.B., Si, H.T., Xiong R.L., Raabe, D.: A novel high manganese austenitic steel with higher work hardening capacity and much lower impact deformation than Hadfield manganese steel. Mater. Des. 55, 798-804 (2014)

[11] Abbasi, M., Kheirandish, S., Kharrazi, Y., Hejazi, J.: On the comparison of the abrasive and wear behavior of aluminum alloyed and standard Hadfield steels. Wear 268, 202-207 (2010).

[12] Zhang, G-S., Xing, J-D., Gao, Y.M.: Impact resistance of WC/Hadfield steel composite and its interfacial characteristics. Wear. 260, 728-734 (2006).

[13] Apostol, M., Vuoristo, T., Kuokkala, V-T.: High temperature high strain rate testing with a compressive SHPB. J. Phys IV. 110, 459-464 (2003).

[14] Terva, J., Teeri, T., Kuokkala, V-T., Siitonen, P., Liimatainen, J.: Abrasive wear of steel against gravel with different rock–steel combinations. Wear. 267, 11, 1821-1831 (2009).

[15] Apostol M., Kuokkala, V-T., Laukkanen, A., Holmberg, K., Waudby, R., Lindroos, M.: High velocity particle impactor – Modeling and experimental verification of impact wear test. World Tribology Congress WTC 2013, Turin, Italy Sept 8-13. 2013.

[16] Sarlin, E., Apostol, M., Lindroos, M., Kuokkala, V.-T., Vuorinen, J., Lepistö, T., Vippola, M.: Impact properties of novel corrosion resistant hybrid structures, Compos Struct. 108, 886-893 (2014).

[17] Petrov, Y., Gavriljuk, V., Berns, H., Schmalt, F.: Surface structure of stainless and Hadfield steels after impact wear. Wear. 260, 687-691 (2006).

[18] Yan, W., Fang, L., Sun, K., Xu, Y.: Effect of surface work hardening on wear behavior of Hadfield steel. Mater. Sci. Eng., A. 460-461, 542-549 (2007).

[19] Lee, W-S., Chen, T-H.: Plastic deformation and fracture characteristics of Hadield steel subjected to high-velocity impact loading, Proceedings of the Institution of Mechanical Engineers, Part C: Journal of Mechanical Engineering Science, 216(2002)10, pp. 971-982.

[20] Karaman, I., Sehitoglu, H., Chumlyakov, Y.I., Maier, H.J., Kireeva, I.V.: Extrinsic stacking faults and twinning in Hadfield manganese steel single crystals. Scripta Mater. 44, 337-343 (2001).

[21] Karaman, I., Sehitoglu, H., Chumlyakov, Y.I., Maier, H.J., Kireeva, I.V.: The Effect of twinning and slip on the Bauschinger effect of Hadfield steel single crystals. Metall Mater Trans A. 696, 32, 695-706 (2001).

[22] Steinmetz, D., Jäpel, T., Wietbrock, B., Eisenlohr, P., Gutierrez-Urrutia, I., Saeed-Akbari, A., Hickel, T., Roters, F., Raabe, D.: Revealing the strain-hardening behavior of twinning-induced
plasticity steels: Theory, simulations, experiments. Acta Mater. 61, 494-510 (2013).

[23] Canadinc, D., Sehitoglu, H., Maier, H.J.: The dense dislocation walls on the deformation response of aluminum alloyed Hadfield steel polycrystals. Mater. Sci. Eng., A. 454-455, 662-666 (2007).

[24] Efstathiou, C., Sehitoglu, H.: Strain hardening and heterogenous deformation during twinning in Hadfield steels. Acta Mater, 58, 1479-1488 (2010).

[25] Zhang, W., Wu, J., Wen, Y., Ye, J., Li, N.: Characterization of different work hardening behavior in AISI 321 stainless steel and Hadfield steel. J. Mater. Sci. 45, 3433-3437 (2010).

[26] Hutchinson, B., Ridley, N.: On dislocation accumulation and work hardening in Hadfield steel. Scripta Mater. 55, 299-302 (2006).

[27] Tsakiris, V., Edmonds, D.V.: Martensite and deformation twinning in austenitic steels. Mater. Sci. Eng., A. 273-275, 430-436 (1999)

[28] Lindroos, M., Kuokkala, V-T., Lehtovaara, A., Kivikytö-Reponen, P.: Effects of strain and strain rate on the abrasive wear behavior of high manganese austenitic steel. Key Eng. Mater. 527, 211-216 (2013).

[29] Abbasi, M., Kheirandish, S., Kharrazi, Y., Hejazi, J.: The fracture and plastic deformation of aluminum alloyed Hadfield steels. Mater. Sci. Eng., A. 513-514, 72-76 (2009)

[30] Khosravifard, A., Moshksar, M.M., Ebrahimi, R.: Mechanical behavior of TWIP steel in high strain rate torsional tests. International Journal of ISSI. 9, 1, 15-19 (2001).

[31] Xiong, Z, Ren, X., Bao, W., Shu, J., Li, S., Qu, H.: Effect of high temperature and high strain rate on the dynamic mechanical properties of Fe-30Mn-3Si-4Al TWIP steel. International Journal of Minerals, Metallurgy, and Materials, 20, 9, 835-841 (2013).

[32] Xiong, Z, Ren, X., Bao, W., Shu, J., Li, S., Qu, H.: Dynamic mechanical properties of the Fe-30Mn-3Si-4Al TWIP steel after different heat treatments. Mater. Sci. Eng., A. 530, 426-431 (2011).

[33] Grässel, O., Krüger, L., Frommayer, G., Meyer, L.W.: High strength Fe-Mn-(Al,Si) TRIP/TWIP steels development – properties – application. Int. J. Plast. 16, 1391-1409 (2000).

[34] Curtze, S., Kuokkala, V-T.: Dependence of tensile deformation behavior of TWIP steels on stacking fault energy, temperature and strain rate. Acta Mater. 58, 5129-5141 (2010).

[35] Curtze, S., Kuokkala, V-T., Oikari, A., Talonen, J., Hänninen, H.: Thermodynamic modeling of the stacking fault energy of austenitic steels. Acta Mater. 59, 1068-1076 (2011).

[36] Pierce, D.T., Jiménez, J.A., Bentley, J., Raabe, D., Oskay, C., Wittig, J.E.: The influence of manganese content to stacking fault and austenite/ε-martensite interfacial energies in Fe-Mn-(Al-Si) steels investigated by experiments and theory. Acta Mater. 68, 238-253 (2014).

[37] Chen, L., Zhao, Y., Qin, X.: Some aspects of high manganese twinning-induced plasticity (TWIP) steels, a review. Acta Metallurgica Sinica, 26, 1, 1-15 (2013).

[38] Tian, X., Zhang, Y.S.: Effect of Cr and Al content on the stacking fault energy in γ-Fe-Mn alloys. Acta Metallurgica Sinica, 16, 3, 211-216 (2003).

[49] Raabe, D., Springer, H., Gutierrez-Urrutia, I., Roters, F., Bausch, M., Seol, J-B., Koyama, M., Choi, P-P., Tsukazi, K.: Alloy design, combinatorial synthesis, and microstructure-property relations for low-density Fe-Mn-Al-C austenitic steels. The minerals, Metals & Material Society. 66, 9, 1845-1856, (2014).

[40] Canadinc, D., Sehitoglu, H., Maier, H.J., Chumlyakov, Y.I.: Strain hardening behavior of aluminum alloyed Hadfield steel single crystals. Acta Mater. 53, 1831-1842 (2005).